Terahertz laser based on dipolaritons

K. Kristinsson,[1] O. Kyriienko,[1,2] and I. A. Shelykh[1,2]
[1]*Division of Physics and Applied Physics, Nanyang Technological University 637371, Singapore*
[2]*Science Institute, University of Iceland, Dunhagi-3, IS-107 Reykjavik, Iceland*
(Received 29 October 2013; published 21 February 2014)

We develop the microscopic theory of a terahertz (THz) laser based on the effects of resonant tunneling in a double quantum well heterostructure embedded in both optical and THz cavities. In the strong-coupling regime the system hosts dipolaritons, hybrid quasiparticles formed by the direct exciton, indirect exciton, and optical photon, which possess large dipole moments in the growth direction. Their radiative coupling to the mode of a THz cavity combined with strong nonlinearities provided by exciton-exciton interactions allows for stable emission of THz radiation in the regime of the continuous optical excitation. The optimal parameters for maximizing the THz signal output power are analyzed.

DOI: 10.1103/PhysRevA.89.023836 PACS number(s): 42.55.Px, 42.50.Ct, 42.65.−k, 71.36.+c

I. INTRODUCTION

The possibility of experimental design of systems of reduced dimensionality has allowed the study of novel types of quasiparticles absent in bulk structures. One of the examples is an indirect exciton, a bound state formed by an electron and a hole confined in spatially separated quantum wells (QWs) [1,2]. Its energy can be effectively tuned by an electric field applied perpendicular to the structure's interface [3]. Due to the small overlap between the wave functions of an electron and a hole, indirect excitons have a much longer radiative lifetime compared to direct excitons, for which an electron and a hole are localized in the same QW [3,4]. Moreover, the presence of an inherent dipole moment strongly enhances exciton-exciton interactions [5,6], making the system of indirect excitons an attractive candidate for the experimental observation of quantum collective phenomena, including excitonic Bose-Einstein condensation (BEC) [7–9].

Another microstructure in which formation of macroscopically coherent states has been reported experimentally is a semiconductor microcavity in the strong-coupling regime, [10,11] in which the optical cavity mode effectively hybridizes with the excitonic mode of a QW embedded in the antinode position. The elementary excitations in this case are cavity polaritons, bosonic quasiparticles containing both light and material fractions. Due to their extremely low effective mass inherited from the cavity photon part a nonequilibrium BEC of polaritons was observed in high quality cavities at liquid nitrogen [12–14] and even at room temperature [15]. Other collective phenomena observed in microcavities include superfluidity [16], Josephson effect [17], optical bistability [18], condensate phase locking [19], formation of quantized vortices, [20] and solitons [21–23].

Indirect excitons and polaritons can be combined in a hybrid structure consisting of a pair of nonequivalent QWs inside a planar microcavity [24–27]. If the band gaps of the two QWs are different, the cavity mode can be tuned to couple resonantly to the excitonic transition in only one of them. In the same time, tuning electron levels of the two QWs into resonance by applying the external electric field, one can achieve the strong tunneling coupling between a direct exciton and a spatially indirect exciton formed by an electron and a hole located in different QWs [Fig. 1(a)]. These strong couplings lead to the appearance of new eigenmodes of the system, which represent three linear superpositions of the cavity photon (C), direct exciton (DX), and indirect exciton (IX) modes. They are called the upper dipolariton (UP), the middle dipolariton (MP), and the lower dipolariton (LP).

It was recently proposed by the authors of the present paper that the dipolariton system can be used as a source of the THz emission in the regimes of both pulsed [28] and continuous [29] excitation. The effect was based on the possibility of achieving huge alterations of the dipole moment in time domain arising from Rabi oscillations between direct and indirect excitons. The important drawback of the approach used in Refs. [28,29] was that the THz emission was considered in a purely classical manner, which excluded the possibility of the analysis of the phenomena related to the possible onset of THz lasing.

In the present paper we account for the quantum nature of the THz emission and propose an experimentally friendly compact scheme of a dipolariton-based laser, operating in a THz domain of frequencies, shown in Fig. 1(b). To enhance the positive feedback for a THz emission we place the double well system inside a high quality THz cavity supporting a mode polarized perpendicular to the QW planes to maximize its coupling to the excitonic dipoles.

The paper is organized as follows. We first introduce the Hamiltonian of the dipolariton system, accounting for the THz mode and its interaction with the excitonic modes, and derive corresponding equations of motion for the fields. We then demonstrate the difference between the bare double QW system, in which oscillations are strongly anharmonic, and the full dipolariton system, where oscillations are harmonic, and show that harmonicity is vital for high stationary occupation of the THz mode. Next we calculate the emission power and investigate its dependence on the THz cavity quality factor Q, finding Purcell enhancement at low Q, and weak dependence past some critical value. Furthermore, we demonstrate coherence-induced superradiance of the emission, which strongly improves the efficiency of the emitter, and address the issue of tunability of the emission frequency.

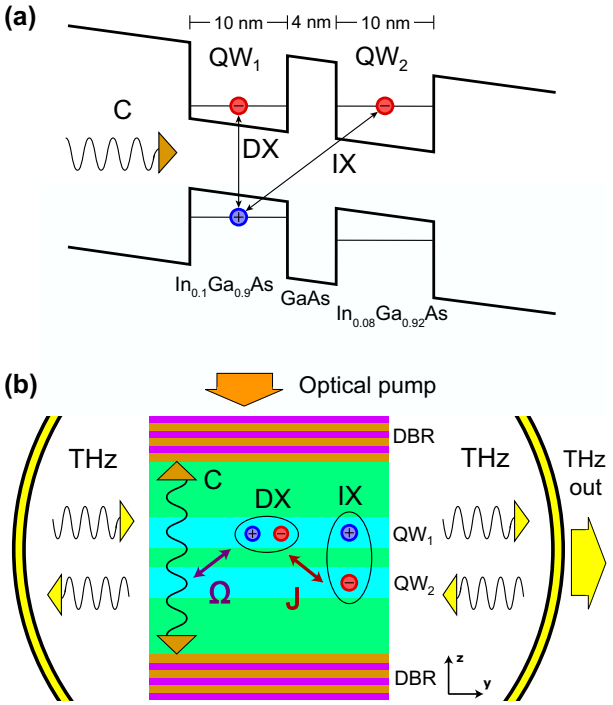

FIG. 1. (Color online) (a) Band diagram of the double QW system. In the presence of the optical microcavity the QW_1 is coupled to the cavity mode. The energy bands are tilted by the applied electric field, bringing the electron levels into resonance. Dimensions and materials of the QWs and the barrier are indicated. (b) Sketch of the dipolariton system in a THz cavity. The QW_1 is where direct excitons (DX) are excited. The electron can tunnel with a rate J to the QW_2, forming indirect excitons (IX). The distributed Bragg reflectors (DBR) provide the confinement of the cavity photon (C), which is strongly coupled to the direct exciton transition with a Rabi frequency Ω, and decoupled from the QW_2. The supplemental cavity hosts a THz photonic mode, which interacts with the exciton dipole moment. The bare double QW system lacks the DBR optical confinement, and therefore the microcavity mode.

II. DOUBLE QUANTUM WELL SYSTEM IN THZ CAVITY

In the first part of the paper we consider the bare double QW system placed inside a THz cavity, assuming an optical cavity being absent [as in Fig. 1(b), but without DBRs]. The upper quantum well (QW_1) hosts direct excitons (DX), excited with a resonant optical pump, with bare energy denoted by $\hbar\omega_D$. The electrons can tunnel to the lower quantum well (QW_2) with a rate J, forming indirect excitons (IX) with energy $\hbar\omega_I$. The QW_2 band gap is different from that of the QW_1, such that the excitonic transitions are out of resonance with the optical excitation. Any formation of QW_2 direct excitons is therefore neglected. Note that the detuning between direct and indirect excitons $\delta_J = \omega_I - \omega_D$ can be tuned by the applied electric field F.

We now put the double QW system inside the THz optical cavity of the wavelength λ_T, with the corresponding frequency ω_T. As the nonzero components of a cavity electromagnetic field are perpendicular to the cavity axis, the THz cavity orientation should be normal to the growth axis of the QWs, so as to couple to the inter-QW dipole transitions.

Using the second quantization formalism we introduce the bosonic creation and annihilation operators for the direct ($\hat{b}^\dagger$, $\hat{b}$) and indirect excitons ($\hat{c}^\dagger$, $\hat{c}$), as well as the THz cavity photons ($\hat{a}^\dagger$, $\hat{a}$). The Hamiltonian of the system can be written as a sum of free energy and tunneling terms, exciton-THz mode interaction, nonlinear Coulomb interaction, and pumping terms,

$$\hat{\mathcal{H}} = \hat{\mathcal{H}}_0 + \hat{\mathcal{H}}_{int} + \hat{\mathcal{H}}_{nonl} + P(t)\hat{b}^\dagger + P(t)^*\hat{b}, \tag{1}$$

where the last two terms describe the coherent optical pumping of the DX mode with intensity $|P(t)|^2$. For the coherent continuous wave (CW) pumping its time dependence has the form $P(t) = P_0 e^{-i\omega_p t}$, where $\hbar\omega_p$ is the pump energy, and P_0 is the amplitude.

The first term reads

$$\hat{\mathcal{H}}_0 = \hbar\omega_T \hat{a}^\dagger\hat{a} + \hbar\omega_D \hat{b}^\dagger\hat{b} + \hbar\omega_I \hat{c}^\dagger\hat{c} - \frac{\hbar J}{2}(\hat{b}^\dagger\hat{c} + \hat{c}^\dagger\hat{b}), \tag{2}$$

and describes the energy of the free mode terms of the THz mode ($\hbar\omega_T$), the direct exciton ($\hbar\omega_D$), and the indirect exciton ($\hbar\omega_I$), as well as the DX-IX tunneling with rate J.

The third term, corresponding to the nonlinear processes, is given by

$$\hat{\mathcal{H}}_{nonl} = \frac{\alpha_1}{2}\hat{b}^\dagger\hat{b}^\dagger\hat{b}\hat{b} + \frac{\alpha_3}{2}\hat{c}^\dagger\hat{c}^\dagger\hat{c}\hat{c} + \alpha_2\hat{b}^\dagger\hat{c}^\dagger\hat{b}\hat{c}. \tag{3}$$

It describes the Coulomb scattering of two direct excitons with interaction constant α_1, two indirect excitons with constant α_3, and the interspecies scattering of a direct and an indirect exciton with constant α_2. The estimation of these constants can be found in Ref. [29].

We can now proceed to account for the interaction between the excitons and the THz cavity, indicated by the second term in Eq. (1).

A. Interaction Hamiltonian

In order to include the interaction between DX, IX, and THz modes we employ the dipole approximation, for which the interaction Hamiltonian can be represented as

$$\hat{\mathcal{H}}_{int} = -\hat{\mathbf{d}} \cdot \hat{\mathbf{E}}, \tag{4}$$

where $\hat{\mathbf{d}}$ is the dipole moment operator of the excitonic system of the double QW, and $\hat{\mathbf{E}}$ is the operator of the electric field corresponding to the THz mode, which in a single mode approximation can be represented as

$$\hat{\mathbf{E}} = \sqrt{\frac{\hbar\omega_T}{2\epsilon V}}(\mathbf{e}\hat{a} + \mathbf{e}^*\hat{a}^\dagger), \tag{5}$$

where ϵ is the electric permittivity, V is the cavity volume, and $\mathbf{e}$ is the THz mode polarization vector.

Using the creation and annihilation operators for the direct and indirect excitons, the dipole moment operator can be written as

$$\hat{\mathbf{d}} = \mathbf{d}_{dd}\hat{b}^\dagger\hat{b} + \mathbf{d}_{ii}\hat{c}^\dagger\hat{c} + \mathbf{d}_{di}\hat{b}^\dagger\hat{c} + \mathbf{d}_{id}\hat{c}^\dagger\hat{b}, \tag{6}$$

where $\mathbf{d}_{jk} = \langle j|\hat{\mathbf{d}}|k\rangle$ are the dipole matrix elements of the double QW exciton states. Because of the cylindrical symmetry of the system we have $\mathbf{d}_{jk} = -e\langle j|\hat{z}|k\rangle\mathbf{e}_z$, where e denotes the elementary charge and the z axis is aligned perpendicular to the QW plane.

We can estimate the indirect exciton dipole matrix element as the electron charge multiplied by an effective electron-hole separation L, $d_{ii} = -e\langle IX|\hat{z}|IX\rangle = -eL$. The direct exciton dipole element d_{dd} arising from the quantum-confined Stark effect can be estimated as

$$d_{dd} = -e\langle DX|\hat{z}|DX\rangle = -24\left(\frac{2}{3\pi}\right)^6 \frac{e^2 F m^* d^4}{\hbar^2}, \quad (7)$$

where F is the applied electric field, m^* is the electron effective mass, and d is the QW width. For a considered $In_{0.1}Ga_{0.9}As$ quantum well the effective mass is $m^* = 0.06m_e$, where m_e is the mass of a free electron. The exciton resonance occurs at $F_0 = 12.5$ kV/cm, and the QWs have a thickness of $d = 10$ nm, separated by a 4-nm barrier. This implies an approximate electron hole separation of $L = 10$ nm. Naturally, the estimated dipole moment of direct exciton in the z direction is much smaller than that of indirect exciton, $d_{dd}/d_{ii} \approx 10^{-3}$, and is neglected in any further consideration. The calculation of d_{di} is presented in the Appendix; for the parameters we consider it can be estimated as $d_{di} \approx 0.17 d_{ii}$.

The dipole transitions couple to the THz cavity field polarized along $\mathbf{e} = \mathbf{e}_z$. Using Eq. (6) the Hamiltonian (4) can be recast as

$$\hat{\mathcal{H}}_{int} = -[g\hat{c}^\dagger\hat{c} + \tilde{g}(\hat{b}^\dagger\hat{c} + \hat{c}^\dagger\hat{b})](\hat{a} + \hat{a}^\dagger), \quad (8)$$

where $g = eL\sqrt{\hbar\omega_T/2\epsilon V}$ and $\tilde{g} = d_{di}\sqrt{\hbar\omega_T/2\epsilon V}$ are the exciton-THz photon coupling constants.

To better understand the origin of the THz emission it is useful to consider the case of zero exciton detuning, $\omega_D = \omega_I$. In this case the eigenmodes of the bare Hamiltonian $\hat{\mathcal{H}}_0$ are the symmetric exciton $\hat{a}_s^\dagger = (\hat{b}^\dagger + \hat{c}^\dagger)/\sqrt{2}$, with energy $\omega_s = \omega_D - J/2$, and the antisymmetric exciton $\hat{a}_a^\dagger = (\hat{b}^\dagger - \hat{c}^\dagger)/\sqrt{2}$, with energy $\omega_a = \omega_D + J/2$. In this basis the interaction Hamiltonian reads

$$\hat{\mathcal{H}}_{int} = -\left[\left(\frac{g}{2} + \tilde{g}\right)\hat{a}_s^\dagger\hat{a}_s + \left(\frac{g}{2} - \tilde{g}\right)\hat{a}_a^\dagger\hat{a}_a\right](\hat{a} + \hat{a}^\dagger) + \frac{g}{2}(\hat{a}\hat{a}_a\hat{a}_s^\dagger + \hat{a}^\dagger\hat{a}_a^\dagger\hat{a}_s) + \frac{g}{2}(\hat{a}\hat{a}_s\hat{a}_a^\dagger + \hat{a}^\dagger\hat{a}_s^\dagger\hat{a}_a). \quad (9)$$

The first line in Eq. (9) describes the interaction of the THz electric field with the static dipole moment of the excitons. The first term of the second line represents the resonant process where a THz photon is absorbed and a lower energy symmetric exciton is excited to the antisymmetric state, as well as the opposite process where an antisymmetric exciton relaxes to the symmetric state, releasing a THz photon (Fig. 2). These terms can be expected to give a major contribution to THz emission. The last term describes the antiresonant processes which are usually disregarded using the rotating wave approximation. However, in our system the transition energies can be in principle comparable to the coupling constant g and these processes cannot in general be neglected.

B. Equations of motion and results

Equations of motion are derived by using the Heisenberg equations for the annihilation operators, and then calculating the expectation value defined as $\langle\hat{a}_i\rangle = \mathrm{Tr}\{\hat{\rho}\hat{a}_i\}$. If we consider the case when occupation numbers are high, the mean-field approximation can be employed, and the following truncation

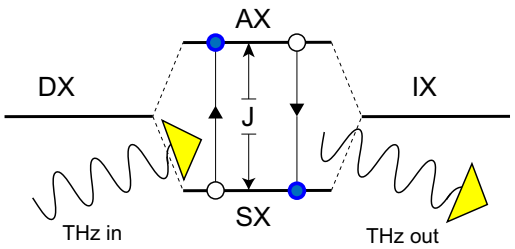

FIG. 2. (Color online) Energy diagram showing the level repulsion between the direct (DX) and indirect excitons (IX) at resonance. New modes, the symmetric (SX) and antisymmetric exciton (AX) arise, split by the tunneling rate J. The resonant processes in the interaction Hamiltonian (9) of THz absorption and emission are shown.

scheme was used to close the set of dynamic equations, $\langle\hat{a}_i\hat{a}_j\cdots\hat{a}_k\rangle \approx \langle\hat{a}_i\rangle\langle\hat{a}_j\rangle\cdots\langle\hat{a}_k\rangle$. To remove references to absolute mode energies, we perform the change of variables $\hat{a}_i \to e^{-i\omega_D t}\hat{a}_i$ ($i = \mathrm{DX}, \mathrm{IX}$). The equations of motion for mean values of operators read

$$\frac{\partial\langle\hat{a}\rangle}{\partial t} = -i\omega_T\langle\hat{a}\rangle + i\frac{g}{\hbar}|\langle\hat{c}\rangle|^2 + i\frac{2\tilde{g}}{\hbar}\mathrm{Re}[\langle\hat{b}\rangle^*\langle\hat{c}\rangle] - \frac{1}{2\tau_T}\langle\hat{a}\rangle, \quad (10)$$

$$\frac{\partial\langle\hat{b}\rangle}{\partial t} = i\frac{J}{2}\langle\hat{c}\rangle + i\frac{2\tilde{g}}{\hbar}\mathrm{Re}[\langle\hat{a}\rangle]\langle\hat{c}\rangle - i\tilde{P}(t) - \frac{i}{\hbar}(\alpha_1|\langle\hat{b}\rangle|^2 + \alpha_2|\langle\hat{c}\rangle|^2)\langle\hat{b}\rangle - \frac{1}{2\tau_{DX}}\langle\hat{b}\rangle, \quad (11)$$

$$\frac{\partial\langle\hat{c}\rangle}{\partial t} = -i\delta_J\langle\hat{c}\rangle + i\frac{J}{2}\langle\hat{b}\rangle + i\frac{2}{\hbar}\mathrm{Re}[\langle\hat{a}\rangle](g\langle\hat{c}\rangle + \tilde{g}\langle\hat{b}\rangle) - \frac{i}{\hbar}(\alpha_2|\langle\hat{b}\rangle|^2 + \alpha_3|\langle\hat{c}\rangle|^2)\langle\hat{c}\rangle - \frac{1}{2\tau_{IX}}\langle\hat{c}\rangle. \quad (12)$$

Lifetimes of the modes have been introduced phenomenologically as $\tau_{DX} = 1$ ns, $\tau_{IX} = 100$ ns, and $\tau_T = Q/\omega_T$, where Q is the quality factor of the THz cavity. After the change of variables the pumping term is written as $\tilde{P}(t) = e^{i\omega_D t}P(t)/\hbar$. Under CW pumping we write $\tilde{P}(t) = \tilde{P}_0 e^{-i\Delta_p t}$, where $\Delta_p = \omega_p - \omega_D$ is the pump detuning from the direct exciton state.

For the numerical analysis we used the same set of parameters as in Ref. [24]. The QW_1 material is $In_{0.1}Ga_{0.9}As$, the QW_2 is grown from $In_{0.08}Ga_{0.92}As$, and the spacer material is GaAs. The well widths are $d = 10$ nm, and the well separation 4 nm, with the tunneling rate set to $\hbar J = 6$ meV [26], which allows us to estimate the effective electron hole separation as $L = 10$ nm. The direct exciton scattering constant is estimated as $\alpha_1 = 6E_b a_B^2/S$ [30], where $a_B = 10$ nm is the direct exciton Bohr radius, and $E_b = 8$ meV is the binding energy. We take $S = 100\ \mu\mathrm{m}^2$ as the system excitation area. The DX-IX interaction constant is taken from Ref. [29], and the indirect exciton scattering constant from Ref. [31]. We consider the THz cavity quality factor to be $Q = 100$ [32,33].

In Ref. [29] it was shown that in the absence of the THz cavity the equations for coupled direct and indirect exciton modes display parametric instabilities in the CW pumping regime. In that work parameters were dressed by the

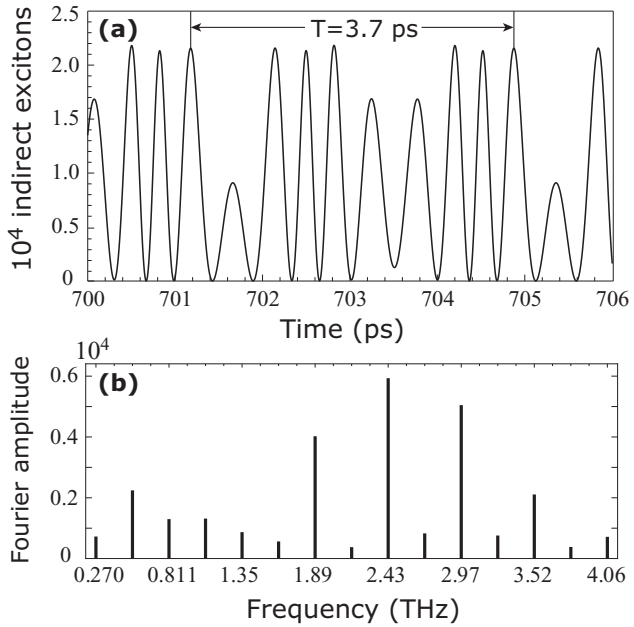

FIG. 3. (a) Occupation number dynamics of the indirect excitons in the double QW system under CW pumping. The exciton detuning is $\hbar\delta_J = 1$ meV, and the pump energy is $\hbar\Delta_p = 1.5$ meV. Pump strength is linearly turned on to $|\tilde{P}_0|^2 = 1.1 \times 10^{29}$ s^{-2} with a short turning on time, driving the system into the parametrically instable regime. The IX occupation number oscillates periodically, but not harmonically. (b) Spectral characteristics of the time dependence shown in (a). The oscillations are distributed between many harmonics, which lowers dramatically the efficiency of THz excitation.

presence of the resonant optical cavity mode, which decreases dramatically the direct exciton effective lifetime. A similar behavior can still be expected here, and as shown in Fig. 3(a), the exciton numbers are indeed found to oscillate periodically, while being strongly anharmonic. The corresponding spectrum of the oscillations is shown in Fig. 3(b). One can see that multiple harmonics have comparable weights, which severely reduces the coupling of the dipole oscillations to the mode of the THz cavity. Consequently, the occupation numbers of THz photons remain extremely small (about $N_{THz} \approx 2$ for the optimal case when cavity mode is tuned in resonance to transition between symmetric and antisymmetric states). This makes the anharmonic case very ineffective for producing single mode THz emission.

III. DIPOLARITON SYSTEM IN A THZ CAVITY

In this section we demonstrate that the presence of the optical cavity tuned close to resonance with excitonic transition can drastically increase the efficiency of the THz lasing. We consider the full dipolariton system, consisting of double QWs embedded in a resonant optical microcavity, with the supplemental THz cavity [see Fig. 1(b)]. In such a system, the eigenstates are linear superpositions of the microcavity photon, direct exciton, and indirect exciton, called lower (LP), middle (MP), and upper (UP) dipolaritons.

A. Hamiltonian and equations of motion

In the dipolariton system, the QW_1 is assumed to be in the strong-coupling regime with the microcavity mode, while the QW_2, with its larger band gap, remains decoupled. The interaction between the direct and indirect excitons, as well as the interaction of the indirect exciton with the THz field, remains unchanged. Denoting the creation operator of the microcavity mode with $\hat{a}_c^\dagger$, the Hamiltonian of the new system is

$$\hat{\mathcal{H}} = \hbar\omega_c \hat{a}_c^\dagger \hat{a}_c + \frac{\hbar\Omega}{2}(\hat{a}_c^\dagger \hat{b} + \hat{b}^\dagger \hat{a}_c) + \hat{\mathcal{H}}_0 + \hat{\mathcal{H}}_{int} + \hat{\mathcal{H}}_{nonl} + P(t)\hat{a}_c^\dagger + P(t)^* \hat{a}_c. \quad (13)$$

The new terms in the first line describe the free propagation of the microcavity photon with energy $\hbar\omega_c$, and the interaction between the microcavity mode and the direct exciton is described by the Rabi frequency Ω. The second line describes the coherent optical pumping, now driving the optical cavity mode.

Equations of motion are derived in the same way as in the previous section. The change of variables is performed slightly differently, as $\hat{a}_i \to e^{-i\omega_c t}\hat{a}_i$ for modes i = C, DX, and IX. The four coupled equations read

$$\frac{\partial\langle\hat{a}\rangle}{\partial t} = -i\omega_T\langle\hat{a}\rangle + i\frac{g}{\hbar}|\langle\hat{c}\rangle|^2 + i\frac{2\tilde{g}}{\hbar}\mathrm{Re}[\langle\hat{b}\rangle^*\langle\hat{c}\rangle] - \frac{1}{2\tau_T}\langle\hat{a}\rangle, \quad (14)$$

$$\frac{\partial\langle\hat{a}_c\rangle}{\partial t} = -i\frac{\Omega}{2}\langle\hat{b}\rangle - \frac{1}{2\tau_C}\langle\hat{a}_c\rangle - i\tilde{P}(t), \quad (15)$$

$$\frac{\partial\langle\hat{b}\rangle}{\partial t} = i\delta_\Omega\langle\hat{b}\rangle - i\frac{\Omega}{2}\langle\hat{a}_c\rangle + i\frac{J}{2}\langle\hat{c}\rangle + i\frac{2\tilde{g}}{\hbar}\mathrm{Re}[\langle\hat{a}\rangle]\langle\hat{c}\rangle - \frac{i}{\hbar}(\alpha_1|\langle\hat{b}\rangle|^2 + \alpha_2|\langle\hat{c}\rangle|^2)\langle\hat{b}\rangle - \frac{1}{2\tau_{DX}}\langle\hat{b}\rangle, \quad (16)$$

$$\frac{\partial\langle\hat{c}\rangle}{\partial t} = i(\delta_\Omega - \delta_J)\langle\hat{c}\rangle + i\frac{J}{2}\langle\hat{b}\rangle + i\frac{2}{\hbar}\mathrm{Re}[\langle\hat{a}\rangle](g\langle\hat{c}\rangle + \tilde{g}\langle\hat{b}\rangle) - \frac{i}{\hbar}(\alpha_2|\langle\hat{b}\rangle|^2 + \alpha_3|\langle\hat{c}\rangle|^2)\langle\hat{c}\rangle - \frac{1}{2\tau_{IX}}\langle\hat{c}\rangle, \quad (17)$$

where $\delta_\Omega = \omega_c - \omega_D$. Furthermore we have introduced the decay of the microcavity mode with a lifetime $\tau_c = 5$ ps.

B. Results

For the calculations in this section we use the same material parameters as before, and choose the Rabi splitting as $\hbar\Omega = 6$ meV [26]. The tunable parameters are chosen as $\hbar\delta_\Omega = -3$ meV and $\hbar\delta_J = 1$ meV. The eigenfrequency of the THz cavity was chosen as $\omega_T/2\pi = 1.74$ THz, and quality factor was taken as $Q = 100$.

Figure 4(a) shows the energy diagram of the dipolariton system, with a vertical line indicating the chosen value of the applied field. The energy of the pump $\hbar\Delta_p = 4.5$ meV lies between the middle and upper dipolariton branches. When the MP mode is populated by the pumping of the system, the corresponding blueshift due to interexciton interactions causes bistability, as shown in Fig. 4(b). For these conditions,

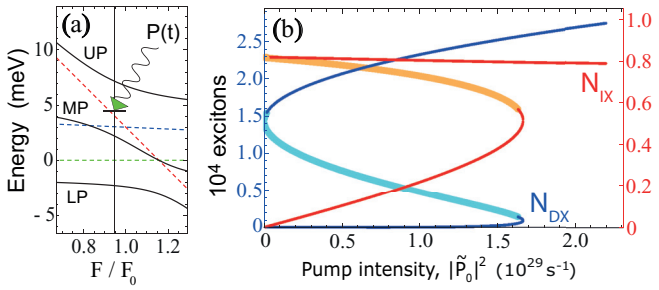

FIG. 4. (Color online) (a) Energy diagram of the dipolariton system, as a function of the applied field F in units of the resonance field F_0. The dashed lines correspond to the bare modes, the photonic (green and flat), the DX (blue), and the IX (red and steep) modes. The diagonalized modes, being the upper (UP), middle (MP), and lower (LP) dipolaritons, are indicated with solid lines. The energy of the pump is identified with a short horizontal line. The vertical line shows the value of the applied field chosen for the calculations. (b) Stability curve under CW pumping for pumping energy $\hbar\Delta_p = 4.5$ meV. The bistability arises here due to the blueshift of the MP mode. The blue curve indicates the DX numbers (left axis), and the red curve is the IX numbers (right axis). Thin segments indicate stability of the population numbers, while the thick lines indicate parametric instability.

parametric instability is achieved as indicated in the plot for a wide range of the pump intensities.

We solved Eqs. (14)–(17) numerically, considering a pump which is linearly turned on, rapidly reaching its stationary value, with transition time being less than 5 ps. This drives the system into the parametrically instable state with oscillations in exciton numbers (see inset to Fig. 5), producing high occupancy of the THz mode. After a transitory period of about ∼400 ps during which a strong outburst of THz radiation occurs, oscillations become harmonic enough for the THz

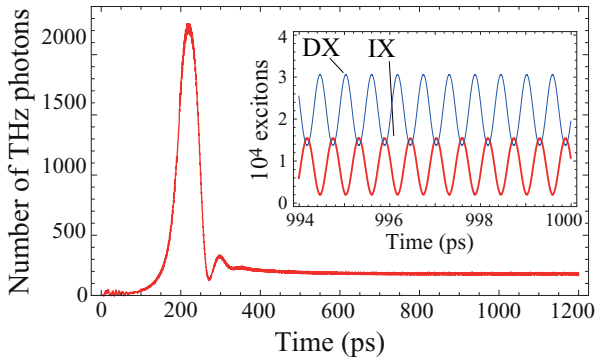

FIG. 5. (Color online) Plot of the occupation number dynamics of a THz cavity with $Q = 100$ coupled to the dipolariton system under CW pumping. The excitonic detuning is $\hbar\delta_J = 1$ meV, the cavity mode detuning is $\hbar\delta_\Omega = -3$ meV, and the relative pump energy is $\hbar\Delta_p = 4.5$ meV, corresponding to the energy-level configuration in Fig. 4(a). The CW pump is rapidly turned on to $|\tilde{P}_0|^2 = 1.1 \times 10^{29}$ s^{-2}. As a result, the system is driven into the parametrically instable regime, provoking oscillations in exciton numbers shown in the inset. For the dipolariton system, these oscillations are harmonic, and result in a stable population of the THz mode $N_{THz} \simeq 200$ photons.

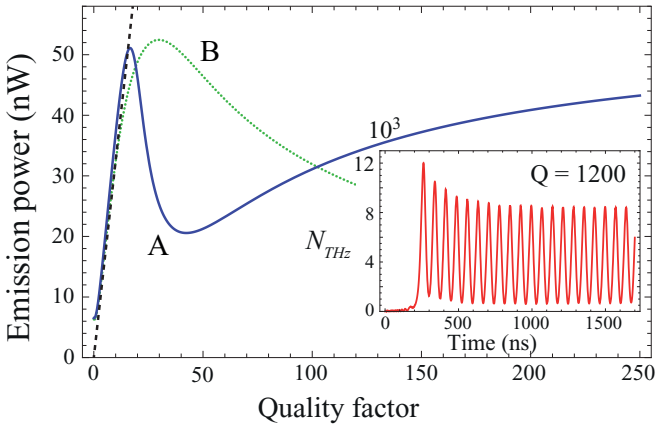

FIG. 6. (Color online) Plot of the time-averaged emission power of THz radiation as a function of the quality factor of the THz cavity. The two lines indicate different pumping strengths, $|\tilde{P}_0|^2 = 1.1 \times 10^{29}$ s^{-2} (pump A, blue line) and $|\tilde{P}_0|^2 = 0.9 \times 10^{29}$ s^{-2} (pump B, green dotted line). The dashed line shows the low Q Purcell effect prediction in Eq. (21) with the IX oscillation amplitude taken as $N_1 = 1.1 \times 10^4$, corresponding to pump A [29]. A peak in emission power is found at $Q = 17$ (A) or $Q = 30$ (B), before dropping due to increased feedback of the THz mode on the indirect exciton. The inset shows the number of THz photons as a function of time for $Q = 1200$ for pump A. For such a high quality factor the number of THz photons is considerably large. The resulting feedback on the excitonic modes is so strong it does not allow for a steady-state solution. Rather, the number of THz photons oscillates, with a period of ≈70 ps, mimicking the output of a Q-switched THz laser.

occupancy to stabilize at the value $N_{THz} \simeq 200$, which is about two orders of magnitude greater than those obtained in the situation where the optical cavity is absent. This drastic increase is connected to the fact that the presence of the optical cavity makes the oscillations of the exciton occupancies highly harmonic (see Fig. 5, inset), which is favorable for monomode emission. This produces constant THz lasing from the system due to the escape of the THz photons out of the cavity. For the chosen parameters the power of the laser can be estimated as $I_0 = N_{THz}\hbar\omega_T/\tau_T \simeq 30$ nW. The dependence of the calculated emission power on the quality factor of the THz cavity is demonstrated in Fig. 6.

C. Discussion

For small Q one can assume that occupancy of the THz mode is relatively small, and its presence only slightly modifies the oscillations between direct and indirect excitons. The equation for the THz mode can be then decoupled from other equations and be considered as a linear differential equation with an external pumping term. If we neglect the effect of the smaller $\tilde{g}$ term we have

$$\frac{\partial\langle\hat{a}\rangle}{\partial t} = -\left(i\omega_T + \frac{1}{2\tau_T}\right)\langle\hat{a}\rangle + i\frac{g}{\hbar}N_{IX}(t), \qquad (18)$$

where the occupancy of the indirect exciton mode can be to a very high precision approximated by a harmonic function,

$$N_{IX}(t) = N_0 + N_1(e^{i\omega t} + e^{-i\omega t})/4, \qquad (19)$$

where N_0 is the average occupancy, and N_1 is the peak-to-valley amplitude of the IX oscillations. The third term is the only resonantly driving term, and we neglect the other two, assuming that the frequency of the excitonic oscillations is in resonance with the eigenfrequency of the THz cavity, $\omega = \omega_T$. The stationary solution of the resulting equation gives for the occupancy of the THz mode

$$N_{THz} = |\langle \hat{a} \rangle|^2 = \frac{g^2 N_1^2 \tau_T^2}{2\hbar^2}, \tag{20}$$

which corresponds to the emission power of

$$I_0^q = \frac{N_{THz}}{\tau_T} \hbar \omega_T = \frac{g^2}{4\hbar} N_1^2 Q. \tag{21}$$

An important attribute of Eq. (21) is that the emitted power is proportional to the square of the indirect exciton number. This corresponds to the *superradiance* effect [34,35], for which the coherence of the quantum-mechanical oscillators causes the emission to increase superlinearly with the number of oscillators. This phenomenon allows reaching high emission power at the engineering stage by up-scaling the device, making it competitive with other schemes of THz generation.

In Refs. [28] and [29] the emission power for the dipolariton system was estimated classically as

$$I_0^c = \frac{N_1^2 d_0^2 \omega_T^4}{48\pi \varepsilon c^3}. \tag{22}$$

By dividing the quantum-mechanical estimate with the classical estimate, one immediately sees that the presence of THz cavity increases the intensity of the emission by the Purcell factor of the system,

$$F_P = \frac{I_0^q}{I_0^c} = \frac{3}{4\pi^2} \frac{\lambda_T^3}{V} Q, \tag{23}$$

where λ_T is a wavelength of THz radiation.

The linear dependence of the emission power on the quality factor given by Eq. (21) is shown by a dotted line in Fig. 6. For the chosen parameters it gives a good approximation for the exact curve for quality factors up to $Q \simeq 17$. Past this point, the emission power experiences a drop due to the increased feedback of the THz mode on excitonic oscillations and then starts to rise again. Changing the pumping strength, we observe that an optimal value of the Q-factor shifts. E.g., for $|\tilde{P}_0|^2 = 0.9 \times 10^{29}$ s^{-2} it is $Q = 30$ (see dotted curve in Fig. 6). In every case the optimal Q factor for THz lasing based on the dipolariton system remains relatively low.

For very large quality factors, $Q \geqslant 10^3$, there appear oscillations in the THz photon occupancy (see the inset to Fig. 6). The oscillations can qualitatively be understood as follows. The high number of THz photons that are quickly excited results in a strong enough feedback to disrupt the resonant oscillations of indirect excitons. As THz photon generation is consequently suppressed, their occupancy decays, and the feedback on the IX mode disappears. At this point exciton oscillations restabilize, again exciting a large number of THz photons. As a steady-state THz occupancy does not develop, it results in the periodical modulation of emission power. This mimics the functionality of a Q-switched laser, with higher peak power than that of the lower Q-factor CW emission. At the onset of these oscillations their period is 73 ps. If the Q factor is further increased the period of these oscillations decreases slightly, e.g., at $Q = 3000$ the period is 64 ps.

Alternatively, the behavior of the system can be understood observing that interaction Hamiltonian (9) couples the quadrature of THz optical mode to the number operators of symmetric and antisymmetric excitons. This is similar to the situation in optomechanical systems [36,37], where parametric instabilities occur for the mechanical mode long lifetime, where the system acts as a saser.

An important question to address is the tunability of the emission. The period of the oscillations of the indirect exciton numbers can be changed by the applied field [28,29], which alters the energy-level structure of the system [see Fig. 4(a)]. Tuning the system in this manner will move the system out of resonance with the THz cavity, lowering the emission power. However, the THz cavity eigenfrequency can be imagined to be alterable, for instance by applying stress to deform the cavity. By simultaneously changing the applied field and the eigenfrequency of the THz cavity, the frequency of emission can be tuned, while staying in resonance.

A surface plot of the emission power is presented in Fig. 7 as a function of the applied field and the THz cavity frequency. The highest emission power follows closely the red solid line, which indicates the frequency of IX oscillations, following the same electric-field dependence as previously observed in Ref. [29]. We find that maximum output power drops in the low electric-field limit (see Fig. 7), caused by the shift of multistability region to the lower pumping strengths, with pump intensity being kept fixed. Consequently, higher values of lasing frequencies can be achieved by tuning the pumping strength. Going beyond the electric-field strength shown in Fig. 7 the output power greatly diminishes, since the system enters the parameter

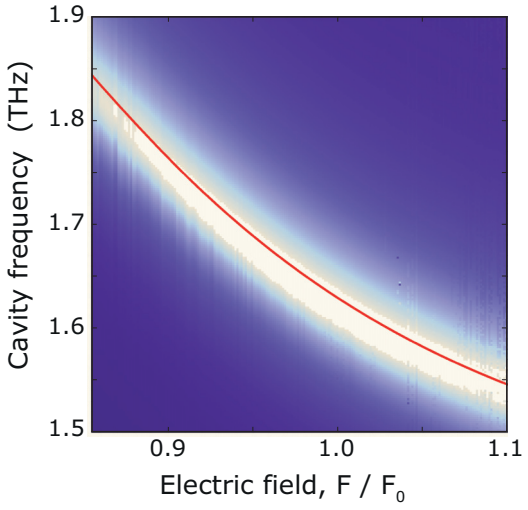

FIG. 7. (Color online) Density plot of the emission power as a function of the applied field and cavity eigenfrequency. The optical cavity detuning is $\hbar\delta_\Omega = -1$ meV, the pump energy is $\hbar\Delta_p = 4.5$ meV, and the pumping strength is $|\tilde{P}_0|^2 = 1.1 \times 10^{29}$ s^{-2}. The quality factor of the THz cavity is $Q = 17$, corresponding to the optimal emission power in Fig. 6. Lighter colors signify higher output power, with the maximum output power following closely the indirect exciton oscillation frequency (red solid line).

regime where indirect exciton number oscillations become anharmonic.

IV. CONCLUSIONS

We have developed a microscopic theory of the terahertz lasing from the dipolariton system. We have shown that in the case of simple double quantum wells embedded in a THz cavity, the tunneling between direct and indirect exciton modes does not lead to stable THz lasing. The presence of an optical cavity strongly coupled with the direct exciton can improve the situation, and stable THz emission becomes possible. The output power of emission was analyzed as a function of THz cavity parameters. In particular, we showed that the THz emission power has a peculiar dependence on THz cavity Q factor, showing that relatively low values are optimal for powerful CW emission. The effect of THz emission superradiance was discussed as a way to achieve high output power. Additionally, we revealed the Q-switched behavior of THz lasing for a high finesse Thz cavity driven by dynamic feedback effects.

ACKNOWLEDGMENTS

We thank T. C. H. Liew for useful discussions on the subject. This work has been supported by FP7 IRSES projects "POLATER" and "POLAPHEN," FP7 ITN project "NOTEDEV" and Tier1 project "Novel polaritonic devices." O.K. acknowledges the support from Eimskip Fund.

APPENDIX: OVERLAP DIPOLE MATRIX ELEMENT

In this section we calculate the dipole matrix element $d_{di} = -e\langle DX|\hat{z}|IX\rangle$. This can be done by calculating the exchange integral between the ground states of two finite potential quantum wells. The time-independent Schrödinger equations for each separate well read as

$$E\psi(z) = -\frac{\hbar^2}{2m^*}\psi''(z) + V(z)\psi(z), \tag{A1}$$

where

$$V(z) = V_0[\theta(-z - d/2) + \theta(z - d/2)], \tag{A2}$$

V_0 is the QW depth, and d is the well width. The ground-state solution to Eq. (A1) reads

$$\psi(z) = \begin{cases} Ae^{\alpha z} & \text{if } z < -L/2, \\ B\cos(kz) & \text{if } |z| < L/2, \\ Ae^{-\alpha z} & \text{if } z > L/2, \end{cases} \tag{A3}$$

where

$$\alpha = \sqrt{2m^*(V_0 - E)}/\hbar, \quad k = \sqrt{2m^*E}/\hbar$$

are parameters found from the lowest k solution to the equation

$$\sqrt{2m^*V_0 - \hbar^2k^2} = \hbar^2k^2\tan(kd/2). \tag{A4}$$

Normalization of the states gives coefficients

$$B = \left(\frac{kd + \sin(kd)}{2k} + \frac{\cos(kd/2)^2}{\alpha}\right)^{-1/2}, \tag{A5}$$

$$A = \cos(kd/2)e^{\alpha d/2}B. \tag{A6}$$

In addition to the parameters in the main text, the valence-band offset between the GaAs bulk and the $In_{0.1}Ga_{0.9}As/In_{0.08}Ga_{0.92}As$ QW is $V_0 = 55$ meV [38]. Finally, the exchange integral can be straightforwardly calculated as

$$\begin{aligned} d_{di} &= \langle DX|(-e\hat{z})|IX\rangle \\ &= -e\int \psi(z)z\psi(z - D)dz \approx -0.17eL, \end{aligned} \tag{A7}$$

where $D = 14$ nm is the distance between the centers of the two QWs.

[1] Yu. E. Lozovik and V. I. Yudson, Zh. Eksp. Teor. Fiz. **71**, 738 (1976) [Sov. Phys.–JETP **44**, 389 (1976)].
[2] L. V. Butov, J. Phys.: Condens. Matter **19**, 295202 (2007).
[3] L. V. Butov, A. L. Ivanov, A. Imamoglu, P. B. Littlewood, A. A. Shashkin, V. T. Dolgopolov, K. L. Campman, and A. C. Gossard, Phys. Rev. Lett. **86**, 5608 (2001).
[4] A. Alexandrou, J. A. Kash, E. E. Mendez, M. Zachau, J. M. Hong, T. Fukuzawa, and Y. Hase, Phys. Rev. B **42**, 9225 (1990).
[5] R. Rapaport, G. Chen, S. Simon, O. Mitrofanov, L. Pfeiffer, and P. M. Platzman, Phys. Rev. B **72**, 075428 (2005).
[6] C. Schindler and R. Zimmermann, Phys. Rev. B **78**, 045313 (2008).
[7] A. A. High, J. R. Leonard, A. T. Hammack, M. M. Fogler, L. V. Butov, A. V. Kavokin, K. L. Campman, and A. C. Gossard, Nature (London) **483**, 584 (2012).
[8] L. V. Butov, C. W. Lai, A. L. Ivanov, A. C. Gossard, and D. S. Chemla, Nature (London) **417**, 47 (2002).
[9] D. Snoke, Science **298**, 1368 (2002).
[10] A. V. Kavokin, J. J. Baumberg, G. Malpuech, and F. P. Laussy, *Microcavities* (Oxford University Press, Oxford, 2007).
[11] I. Carusotto and C. Ciuti, Rev. Mod. Phys. **85**, 299 (2013); H. Deng, H. Haug, and Y. Yamamoto, *ibid.* **82**, 1489 (2010).
[12] J. Kasprzak, M. Richard, S. Kundermann, A. Baas, P. Jeambrun, J. M. J. Keeling, F. M. Marchetti, M. H. Szymanska, R. Andre, J. L. Staehli, V. Savona, P. B. Littlewood, B. Deveaud, and Le Si Dang, Nature (London) **443**, 409 (2006).
[13] R. Balili, V. Hartwell, D. Snoke, L. Pfeiffer, and K. West, Science **316**, 1007 (2007).
[14] C. Schneider, A. Rahimi-Iman, Na Young Kim, J. Fischer, I. G. Savenko, M. Amthor, M. Lermer, A. Wolf, L. Worschech, V. D. Kulakovskii, I. A. Shelykh, M. Kamp, S. Reitzenstein, A. Forchel, Y. Yamamoto, and S. Hofling, Nature (London) **497**, 348 (2013).

[15] S. Christopoulos, G. Baldassarri Höger von Högersthal, A. J. D. Grundy, P. G. Lagoudakis, A. V. Kavokin, J. J. Baumberg, G. Christmann, R. Butté, E. Feltin, J.-F. Carlin, and N. Grandjean, Phys. Rev. Lett. **98**, 126405 (2007).
[16] A. Amo, D. Sanvitto, F. P. Laussy, D. Ballarini, E. del Valle, M. D. Martin, A. Lemaitre, J. Bloch, D. N. Krizhanovskii, M. S. Skolnick, C. Tejedor, and L. Vina, Nature (London) **457**, 291 (2009).
[17] K. G. Lagoudakis, B. Pietka, M. Wouters, R. Andre, and B. Deveaud-Pledran, Phys. Rev. Lett. **105**, 120403 (2010).
[18] A. Baas, J. Ph. Karr, H. Eleuch, and E. Giacobino, Phys. Rev. A **69**, 023809 (2004).
[19] P. Cristofolini, A. Dreismann, G. Christmann, G. Franchetti, N. G. Berloff, P. Tsotsis, Z. Hatzopoulos, P. G. Savvidis, and J. J. Baumberg, Phys. Rev. Lett. **110**, 186403 (2013).
[20] K. G. Lagoudakis, F. Manni, B. Pietka, M. Wouters, T. C. H. Liew, V. Savona, A. V. Kavokin, R. André, and B. Deveaud-Plédran, Phys. Rev. Lett. **106**, 115301 (2011).
[21] M. Sich, D. N. Krizhanovskii, M. S. Skolnick, A. V. Gorbach, R. Hartley, D. V. Skryabin, E. A. Cerda-Méndez, K. Biermann, R. Hey, and P. V. Santos, Nat. Photon. **6**, 50 (2012).
[22] R. Hivet, H. Flayac, D. D. Solnyshkov, D. Tanese, T. Boulier, D. Andreoli, E. Giacobino, J. Bloch, A. Bramati, G. Malpuech, and A. Amo, Nat. Phys. **8**, 724 (2012)
[23] O. A. Egorov, D. V. Skryabin, and F. Lederer, Phys. Rev. B **82**, 165326 (2010).
[24] G. Christmann, A. Askitopoulos, G. Deligeorgis, Z. Hatzopoulos, S. I. Tsintzos, P. G. Savvidis, and J. J. Baumberg, Appl. Phys. Lett. **98**, 081111 (2011).
[25] G. Christmann, C. Coulson, J. J. Baumberg, N. T. Pelekanos, Z. Hatzopoulos, S. I. Tsintzos, and P. G. Savvidis, Phys. Rev. B **82**, 113308 (2010).
[26] P. Cristofolini, G. Christmann, S. I. Tsintzos, G. Deligeorgis, G. Konstantinidis, Z. Hatzopoulos, P. G. Savvidis, and J. J. Baumberg, Science **336**, 704 (2012).
[27] K. Sivalertporn, L. Mouchliadis, A. L. Ivanov, R. Philp, and E. A. Muljarov, Phys. Rev. B **85**, 045207 (2012).
[28] O. Kyriienko, A. V. Kavokin, and I. A. Shelykh, Phys. Rev. Lett. **111**, 176401 (2013).
[29] K. Kristinsson, O. Kyriienko, T. C. H. Liew, and I. A. Shelykh, Phys. Rev. B **88**, 245303 (2013).
[30] F. Tassone and Y. Yamamoto, Phys. Rev. B **59**, 10830 (1999).
[31] O. Kyriienko, E. B. Magnusson, and I. A. Shelykh, Phys. Rev. B **86**, 115324 (2012).
[32] Y. Chassagneux, R. Colombelli, W. Maineult, S. Barbieri, H. E. Beere, D. A. Ritchie, S. P. Khanna, E. H. Linfield, and A. G. Davies, Nature (London) **457**, 174 (2009).
[33] A. J. Gallant, M. A. Kaliteevski, D. Wood, M. C. Petty, R. A. Abram, S. Brand, G. P. Swift, D. A. Zeze, and J. M. Chamberlain, Appl. Phys. Lett. **91**, 161115 (2007).
[34] R. H. Dicke, Phys. Rev. **93**, 99 (1954).
[35] J. G. Bohnet, Z. Chen, J. M. Weiner, D. Meiser, M. J. Holland, and J. K. Thompson, Nature (London) **484**, 78 (2012).
[36] S. Aldana, C. Bruder, and A. Nunnenkamp, Phys. Rev. A **88**, 043826 (2013).
[37] O. Kyriienko, T. C. H. Liew, and I. A. Shelykh, Phys. Rev. Lett. **112**, 076402 (2014).
[38] H.-P. Komsa, E. Arola, and T. T. Rantala, Appl. Phys. Lett. **92**, 262101 (2008).